ARCHIVIO ISTITUZIONALE
DELLA RICERCA

Alma Mater Studiorum Università di Bologna
Archivio istituzionale della ricerca

A Numerical Methodology to Test the Lubricant Oil Evaporation and Its Thermal Management-Related Properties Derating in Hydrogen-Fueled Engines

(Article begins on next page)

This is the final peer-reviewed accepted manuscript of:

Terms of use:

A numerical methodology to test the lubricant oil evaporation and its thermal management-related properties derating in hydrogen fuelled engines.

Author, co-author
Affiliation

Abstract

Due to the incoming phase out of fossil fuels from the market in order to reduce the carbon footprint of the automotive sector, hydrogen fuelled engines are candidate mid-term solution. Thanks to its properties, hydrogen promotes flames that poorly suffer from the quenching effects towards the engine walls. Thus, emphasis must be posed on the heat-up of the oil layer that wets the cylinder liner in hydrogen fuelled engines. It is known that motor oils are complex mixtures of a number of mainly heavy hydrocarbons (HCs) however, their composition is not known a-priori. Simulation tools that can support the early development steps of those engines must be provided with oil composition and properties at operation-like conditions. The Authors propose a statistical inference-based optimization approach for identifying oil surrogate multi-component mixtures. The algorithm is implemented in Python and relies on the Bayesian optimization technique. As a benchmark, the surrogate for the SAE5W30 commercial multigrade oil has been determined. Then, this multicomponent surrogate and a SAE5W30 pseudo-pure are compared by means of an oil film model which accounts for oil heat exchange with the cylinder wall and the gases from hydrogen combustion, and its evaporation. The results in terms of oil film temperature, viscosity and thickness under hydrogen-engine boundaries are evaluated. Analyses reveal that the optimized multicomponent mixture behavior is more realistic and can outperform the pseudo-pure approach when the oil phase change and the oil in-cylinder presence must be considered.

Keywords: Lubricant Oil, Hydrogen, Internal Combustion Engine, Evaporation, Mass and Heat Transfer, Model.

Introduction

Nowadays increasing the energy efficiency of Internal Combustion Engines (ICEs) is mandatory in order to both avoid fossil fuel wasting and slow down the greenhouse gases-induced global warming. Over the last decades, several different technological solutions have been adopted focusing on improving the indicating efficiency and the thermal efficiency by reducing the pump losses at low load and limiting the knock tendency at high load [1-7]. Recently, due to the emphasis posed on the zero-carbon emission goal at the vehicle tailpipe, thus the phase out of fossil fuels from the market, the retrofit of ICEs to fit the combustion of hydrogen (H2) is gaining significant attention considering both the stand-alone power unit and the hybridization with fuel cells options [8]. Regardless of the specific technology, it is known that oil is crucial in the thermal management of the ICE as a key player in lubrication, protection, and cooling. As a consequence, mapping the behavior of the oil in order to assess the

derating of its properties (e.g., surface tension, viscosity) is fundamental for the analysis of the engine reliability and thermal efficiency under those new operation conditions.

In the framework of hydrogen fuelled engines, the oil layer upon the cylinder wall suffers from issues that are typical of hydrogen combustion. For the sake of comparison, Table 1 summarizes some key combustion related properties of hydrogen against those of gasoline. On the one hand, the use of hydrogen ensures: i) increased thermal efficiency allowing ultra-lean mixtures ($\lambda = 2$) thanks to the extended flammability limits; ii) increased indicating efficiency due to the faster combustion associated to the greater flame speed, which promotes combustion events closer to the ideal constant-volume instantaneous combustion of the Otto thermodynamic cycle; iii) lack of fuel-derived soot emission and carbon dioxide. On the other hand, due to the hydrogen properties, this technology shows some shortcomings to be handled [9-11]. Indeed, because of the higher lower heating value per mass, the higher combustion temperature when burning hydrogen may enhance the NOx production. The super low auto-ignition energy exposes the engine to the likelihood of intense pre-ignition phenomena, with concerns on the mechanical safety. Due to the presence of large amount of product water, the backflow of some exhausts may cause the condensation of such water inside the intake port. This water may be re-entered inside the cylinder leading to the oil properties degradation. Furthermore, the shorter quenching distance promotes the flame front propagation towards the engine walls up to the attack against them. As a result, the heat exchange between oil and the end-gases due to convection and oil and the flame due to the radiative mechanism leads to temperature of the lubricant above the typical oil evaporation temperature, which is around 200 °C.

Table 1. Comparison between commercial gasoline and hydrogen combustion properties. Data taken from Ref. [9].

Property	Commercial gasoline	Hydrogen
Flammability limit	1.3-7.1 %vol in air	4-75 %vol in air
Laminar flame speed	0.37-0.43 m/s	1.85 m/s
Minimum ignition energy	5.5 x 10-4 J	1.9 x 10-5 J
Quenching distance	2.84 mm	0.64 mm

Since lubricant oil is mainly composed of hydrocarbon molecules and it is characterized by large chemical reactivity (low ignition delay time and ignition temperature), ignition spots can be triggered inside the cylinder leading to the formation of soot [12]. In [13] Miller et al.

modified a diesel engine in order to fit hydrogen fuel combustion, then, they performed the particles analysis (number, size, morphology, type) of the exhaust gases by means of different techniques. From the experimental measurements, the Authors observed the presence of soot, which must be oil-derived due to the lack of fossil fuel supply. The Authors stated that soot is formed due to the gas-to-particle conversion of the evaporated burning oil by nucleation and vapor deposition. Another hydrogen-related concern is the oil properties derating due to the reaction of the activated hydrogen with lubricant and additives. In [14] Garcia et al. performed the analysis of the lubricant oil and of the smoke opacity in a compression ignition engine run in dual-fuel conditions with diesel fuel directly injected inside the chamber, and hydrogen fuel supplied via the intake port. Different load conditions and hydrogen flow rate values were tested. After the oil pollution analysis, the Authors detected an increased presence of metallic components such as iron, copper, aluminum, chromium likely due to the hydrogen-oil interaction which has led to grater wear. Furthermore, a maximum viscosity reduction of oil around 25% was observed as the hydrogen supply rate increased. Moreover, it must be considered that hydrogen combustion produces larger amount of water with respect to fossil fuels, being water the only combustion product if hydrogen is adopted as a fuel. Since the current engine technology was not developed to fit such water quantity during operations, increased oil emulsion, parts wear and corrosion were promoted. In light of those issues, some challenges must be faced in order to make this technology competitive and mature, e.g., put care in designing the turbo-match, use of high boost pressure, application of hydrogen direct injection in order to ensure an ultra-lean mixture and limit the oil-hydrogen interaction; advanced combustion modes, laser ignition, in order to improve combustion stability and repeatability at highly dilution (high exhaust recirculation amount, high lambda) even at low-mid load; dedicated SCR (Selective Catalyst Reduction) systems for the NOx treatment [9-11].

Since there are significant concerns on the influence of hydrogen fuel on the lubricant oil in terms of thermal management and reliability, more emphasis must be posed in predicting the oil behavior and phase change in H2 engine solutions. Simulations accounting for the engine oil behavior have been scarcely investigated in the current state of the art. In [15] Yu and Min proposed a one-dimensional time-varying diffusion model for the liquid fuel film – oil dilution and an absorption/desorption mode for gaseous fuel in oil applied to the warm-up conditions of a reference experimental SI engine. The model can fit an isothermal system of two fluids (fuel and oil considered as pseudo-pure), the fuel phase change was allowed at the liquid-gas interface. In [16] Zhang et al. applied the concept proposed by Yu and Min aiming at the investigation of the oil-induced pre-ignition in SI engines at full load. In order to accomplish the task, the Authors enrich the Yu and Min oil-fuel dilution proposal with the modelling of the heat transfer considering both the heat conduction between cylinder wall and liquid phases, and the heat conduction through the oil-fuel liquid film. Furthermore, the Authors implemented the liquid fuel as a multicomponent mixture with different diffusion rate for each component. In [17] Mariani et al. the Authors presented an improved version of the model by Zhang for the oil-fuel dilution analysis by enhancing the features of the diffusion model with the use of a new hybrid deep neural networks methodology for predicting the binary diffusion coefficient between engine oils and typical gasoline fuels. Furthermore, additional care was placed in the mixing rules for the calculation of the oil-fuel mixture properties depending on both temperature and composition. It must be underlined that the described literature models do not account for the oil evaporation and oil vapor properties since this phase change cannot be achieved under standard engine operations.

As far as hydrogen fuel is concerned, oil evaporation must be implemented. Engine oils are mixtures of several components, if new oil is considered, the components are mainly HCs, from the lighter ones (C14-C16) to the heavier ones (C40-C50). On the other hand, if aged oil is considered, a significant presence of aromatics can be observed [18]. The composition of engine oils is not known a-priori, and even though, the number of components would be a limiting factor for fast computation with respect to the typical response time of one-dimensional models. Furthermore, it is underlined that adopting a pseudo-pure liquid approach with average properties, would lead to poor results in the estimation of oil sourced in-cylinder HCs.

In light of the above, detailed simulation analyses involving oil behavior for thermal and reliability aspects in H2-fuelled engines, require the identification of a proper surrogate mixture of the lubricant. Surrogates are mixtures of different known pure molecules whose composition (the number and the percentage value of each component) is able to capture a set of target properties of the real fluid, namely the lubricant oil. In the current literature, the surrogate mixture approach has been widely applied to identify mixtures of known HCs and oxygenates able to match spray properties [19] and combustion properties [20] of commercial gasolines. However, scarce attention has been paid to the formulation of surrogate mixtures for engine oils. This modeling approach allows increased accuracy in different modeling areas in which the oil interaction with other fluids plays a key role e.g.: i) oil evaporation and diffusive burning with the in-cylinder air, in which the identification over the evaporated species is fundamental for the choice of the kinetics mechanisms; ii) product water from hydrogen combustion absorption/desorption in the oil layer, in which the saturation threshold, thus, the presence of water in the oil pan, strongly depends on the oil composition. Those simulations can help the early development steps of hydrogen engines and can provide insights on the effects of hydrogen combustion such as oil pollution, hydrogen diffusive combustion inside the crevices, presence of liquid water inside the pan.

This work deals with the implementation and test of a machine learning-based algorithm which relies on the Bayesian statistical inference for the optimization of oil surrogate mixture composition. The aim is to provide a tool able to return the mixture (number, type and percentage) of hydrocarbons that can mimic key aspects of real engine oils. This mixture can be then used in simulations code that are based on the oil properties and behavior. The methodology was based on a previous work of some of the present Authors [21]. A set of pure molecules to be used to perform mixture options was selected and a set of target properties of oils to be captured was chosen. In this work, density, viscosity, specific heat, thermal conductivity, flash point, normal boiling temperature were selected according to simulation-oriented considerations that will be discussed in the next sections. The activity has been divided into two steps: i) the algorithm has been used to determine the proper surrogate for the SAE-5W30 multigrade commercial oil. Firstly, a sensitivity analysis of the algorithm to the size of the pure molecules has been conducted by reducing the number of components available to design the surrogate (20, 15, 10, 8 components were tested). Then, the minimum number was adopted to search the optimum mixture considering two reference temperatures at which the properties has been estimated (293 K, 373 K); ii) The SAE-5W30 surrogate multicomponent mixture is then used in a code [22] simulating the oil film behavior at H2-fuelled engine conditions in comparison with a SAE5W30 pseudo-pure. The oil film thickness reduction due to the combustion-induced evaporation have been observed against time for both the simulation approaches. Furthermore, the temperature and the viscosity of the oil layer along the thickness have been analyzed.

Methodology

Properties and components description

As previously mentioned, the lower flame quenching distance from the cylinder liner typical of a hydrogen fuelled ICE promotes higher walls and lubricant layer temperatures, thus possibly enhancing lubricant evaporation and derating. A preliminary analysis is conducted in order to establish a set of key SAE5W30 engine oil properties, which are involved in the mass and heat transfer and mass evaporation phenomena. Furthermore, it is crucial for these properties to ensure a defined range of change with temperature in order to guarantee the lubricant operation under safe and expected conditions. Firstly, a literature review is performed in order to define the components that can fit an engine oil-like mixture. As a consequence, a pure fluids database is defined to feed the optimization routine. Then, the properties of the pure hydrocarbons and the corresponding mixing rules are discussed.

Pure components choice

A deep literature review has been performed to determine the proper composition options and the number of pure components available to define mixtures which mimic the oil behavior. First, the quality of the pure components is addressed. Various works highlight that unused oil is for the most part composed of unbranched hydrocarbons, i.e., n-alkanes (or naphtenes). Polycyclic Aromatic Hydrocarbons (PAHs) are detected only in used engine oil and may contribute to exhaust particulate PAH emissions during both firing and motored operations. In particular, Lu et al. [23] have conducted an experimental campaign by means of Gas Chromatography (GC) to understand the composition differences in both used and unused engine oil, finding that PAH were present only in used engine oils. Also, Cvengroš et al. [24] used proton nuclear magnetic resonance (H NMR) spectroscopy through Hbay methodology to determine the PAH contents in 15 selected samples of unused engine oil, which were even lower with respect to the regulations. Williams et Al. analyzed the PAH presence in engine oil with dependence on oil aging. They found that PAH builds up in used lubricating oil with age and that the PAH are derived from unburnt fuel directly [18]. Wang et Al. [25] performed a high-resolution GC analysis and found that the unused base lubricant oil under analysis was composed by normal paraffines from C20 to C34, while Lu et al. [23] determined that also lighter, such as C15, and heavier, such as C40, components can be found in the unused base lubricant oil.

In light of the above, the Authors consider a pure components database made by normal paraffines ranging from C5 to C45 to model an unused lubricant oil, as shown in Table 2.

Properties

Among the many different functions fulfilled by engine oil, this work is mainly focused on two needs: i) moving parts lubrication, (e.g., piston upward-downward along the cylinder wall to reduce frictions and wear); ii) dissipation of the heat generated due to combustion. A suitable set of lubricant oil properties has been chosen to evaluate the oil degradation with dependence on the system temperature and to model the mass and heat physical phenomena. These properties include the liquid phase viscosity, density, specific heat capacity, thermal conductivity, flash point, normal boiling temperature.

Generally, the design viscosity grade depends on the engine manufacturing tolerances. A higher viscosity grade oil tends to easily

adhere to the walls and to compensate for the clearance deterioration due to engine aging, while its resistance to flow may affect its recirculation and the engine efficiency. On the other hand, a low viscosity grade oil is better recirculated and easily flows through the engine parts while it may leak, letting the surfaces dry and enhancing friction and wear. Simulation-wise, the mean oil layer viscosity and the viscosity of the oil components are required to evaluate the mass diffusion coefficients (as it will be shown later). Also, it is of interest to measure its degradation caused by the high in-cylinder temperature. Viscosity (μ) is evaluated by means of equation 1 [26]:

$$\log \mu = B \left(\frac{1}{T} - \frac{1}{T_O} \right); \qquad (1)$$

Table 2. Pure components database used in the optimization algorithm.

pentane	C5H12	nona-decane	C19H40	tri-triacontane	C33H68
hexane	C6H14	ei-cosane	C20H42	tetra-triacontane	C34H70
heptane	C7H16	henei-cosane	C21H44	penta-triacontane	C35H72
octane	C8H18	do-cosane	C22H46	hexa-triacontane	C36H74
nonane	C9H20	tri-cosane	C23H48	hepta-triacontane	C37H76
decane	C10H22	tetra-cosane	C24H50	Octa-triacontane	C38H78
un-decane	C11H24	penta-cosane	C25H52	nona-triacontane	C39H80
do-decane	C12H26	hexa-cosane	C26H54	tetra-contane	C40H82
tri-decane	C13H28	hepta-cosane	C27H56	hente-tracontane	C41H84
tetra-decane	C14H30	octa-cosane	C28H58	dote-tracontane	C42H86
penta-decane	C15H32	nona-cosane	C29H60	tri-tetracontane	C43H88
hexa-decane	C16H34	tria-contane	C30H62	tetra-tetracontane	C44H90
hepta-decane	C17H36	hentria-contane	C31H64	penta-tetracontane	C45H92
octa-decane	C18H38	dotria-contane	C32H66		

In equation 1 viscosity is expressed in cP, T is the temperature in K. T_O and B are constants which accounts for the viscosity dependency on the hydrocarbon carbon number.

Density (ρ) is required to determine the mass involved in the studied physical phenomena in the simulation model. As for viscosity, density is used for calculating the binary mass diffusion coefficients as well. Density depends on temperature, and it influences lubricant oil performance. For instance, a high-density lubricant oil is less likely to

penetrate engine areas which are hard to reach. Though, low-density oil tends to evaporate more (especially in a hydrogen fuelled engine) increasing oil consumption. Density for pure normal alkanes is evaluated through the equation 2 [27]:

$$\rho = -3.469 + 0.0006896\,A + \frac{B}{M_w + P} + ..$$

$$+(M_w + P)\,C + D + E; \tag{2}$$

In equation 2 density is in g/cm³, P is the pressure of the system expressed in MPa, M_w is the molecular weight of the normal alkane expressed in g/mol. A, B, C, D, E depend on pressure and temperature.

Liquid specific heat capacity (C_p) and thermal conductivity (k) are used to model the thermal diffusion coefficient and the evaporation rate of the pure components, thus allowing to update the oil layer and the gas temperatures by the heat transfer and the coolant effect of the evaporating mixture. Specific liquid heat capacity is modelled by means of equation 3 [28]:

$$C_P = a_1 + (a_{21}\alpha + a_{22}\alpha^2)\,T + (a_{31}\alpha + a_{32}\alpha^2)\,T^2; \tag{3}$$

where $a_1 = 24.5\,(a_{11}\alpha + a_{12}\alpha^2)$ for temperatures above 200 K, which is always true under the considered working conditions, α is defined as the number of atoms in a molecule divided by the molecular mass and $a_{11}, a_{12}, a_{21}, a_{22}, a_{31}, a_{32}$ are universal coefficients (-0.3416, 2.2671, 0.1064, -0.3874, -9.8231 x 10^{-5}, 4.182 x 10^{-4}, respectively).

Liquid thermal conductivity is modelled with equation 4 from Perry's Chemical Handbook [24]:

$$k_L = C\rho M_w{}^n \left(\frac{3 + 20(1 - T_r)^{2/3}}{3 + 20\left(1 - \frac{293.15}{T_c}\right)^{2/3}} \right); \tag{4}$$

Liquid thermal conductivity is in W/m K, C and n are constants equal to 1.001 and $1.811 \cdot 10^{-4}$ respectively for straight chain hydrocarbons, ρ_M is the molar density at 293.15 K expressed in kmol/m³, T_r and T_c are the reduced ($T_r = T/T_c$) and the critical temperatures.

Then, flash point (T_F) is considered. As previously mentioned, the lower hydrogen flame quenching distance with respect to the cylinder line may promote lubricant oil evaporation or, in the worst case, ignition of the lubricant oil vapor: within these regards, lubricant flash point is calculated by means of equation 5 [29]:

$$T_{F,mix} = \frac{2414}{6.1188 + \log_{10}(I_{mix})} - 230.56; \tag{5}$$

where I_{mix} is the index for the hydrocarbons' mixture which is calculated once the flash point index (equation 6) and the volume fractions of the component in the mixture are known.

$$\log_{10}(I) = -6.1188 + \frac{2414}{T_F + 230.56}; \tag{6}$$

The T_F of the pure hydrocarbons are available in the *ChemSpider* [30] library.

Finally, the normal boiling point of the lubricant oil is calculated with a dedicated sub-model, being evaporation properties not additive. The sub-model is based on the zero-dimensional distillation model developed by Mariani et al. [17], which is based on the works of Slavinskaya et al. [31] and Abianeh et Al. [32], allowing to evaluate the first boiling temperature by means of a pure thermodynamic model. This thermodynamic model relies on the classical Vapor-Liquid Equilibrium (VLE) bubble point temperature problem. Since the mixture in non-ideal, the VLE is expressed through the equality between liquid and vapor fugacity instead of the Raoult's law. Mixture fugacity is estimated with the dual-fugacity method by correlating the fugacity with the partial pressure as equation 7 shows:

$$\varphi_{V,i} \cdot y_i \cdot p = \varphi_{L,i} \cdot x_i \cdot p; \tag{7}$$

where $\varphi_{V,i}$ and $\varphi_{L,i}$ are the fugacity coefficients for the vapor and liquid phases, p is the pressure, y_i and x_i are the moles fraction of the i-th component in the vapor and liquid, respectively. Fugacity coefficients (equation 8) are calculated through the Soave-Redlich-Kwong (SKR) cubic equation of state [33]:

$$\varphi_i = exp[\beta_i(Z - 1) - \ln(Z - B) + ..$$

$$-\frac{A}{B}(\alpha_i - \beta_i) \cdot ln\left(1 + \frac{B}{Z}\right)]; \tag{8}$$

In equation 8, Z is the compressibility factor, A, B, α, β are coefficients that include constants, equilibrium pressure, temperature and the two SKR mixture parameters a and b.

This sub-model is validated against the experimental data from the work of Bruno and Smith [34]. The Authors showed that the vapor rise temperature corresponds to the initial boiling temperature. The normal boiling temperature of two different surrogates, namely *Aachen* and *modified Aachen* as reported in the reference. Table 3 shows that the calculated normal boiling temperatures, at the specified pressures. Table 3 last row refers to the NBTs calculated by means of the methodology presented in this work, which differ from the onset temperatures of around ≈ 10 K and of less than 7 K for the *Aachen* and for the modified Aachen surrogates, respectively.

In this work, the SAE5W30 multigrade engine oil was considered as a test benchmark. In particular, the *Mathworks Simscape* library is used to determine the properties that have been chosen as target. Three different temperatures are investigated to mimic a low, medium and high load engine and lubricant oil operating conditions. Table 4 sums up these values for clarity.

Surrogate	Aachen	modified Aachen
Composition	80% decane	80% dodecane
	20% 1,2,4-trimethylbenzene	20% 1,2,4-trimethylbenzene
Pressure (Pa)	83740	83230
Onset temp. (K)	408.75	457.25
Experimental NBT (K)	445.35	470.35
Calculated NBT (K)	434.66	463.69

Table 4. Selected target properties and temperatures to perform the surrogates' optimization.

Properties	@293 K	@313 K	@373 K
Density ($kg\ m^{-3}$)	852.1	840.1	804.1
Viscosity (cP)	92.5	49.4	10.3
Heat capacity ($J\ kg^{-1}\ K^{-1}$)	1984.0	2056.0	2305.0
Therm. conductivity ($W\ m^{-1}\ K^{-1}$)	0.133	0.129	0.117
Flash point temp. (K)	503.15	503.15	503.15
Normal boiling temperature (K)	593.15	593.15	593.15

Oil surrogate optimization

Standard root-finding algorithms cannot fit optimization problems properly if the solution domain is large and if the bond between input-output is highly non-linear. It must be considered that for the oil surrogate problem, the solution domain size is the number of pure molecules available to fill the surrogate mixture. Furthermore, the mixing rule for the thermal conductivity and the custom sub-model for the normal boiling temperature are strongly non-linear. Therefore, different techniques had to be implemented. The present Authors adopted an optimization approach based on the Bayesian statistical inference in order to guide the maximum search. The Bayesian algorithm is charged to search the global maximum of the objective function F in the surrogate mixture composition domain X up to the definition of the optimal oil surrogate x^* so that $x^* = \text{argmax } F(x)_{x \in X}$. The Bayesian search relies on the Gaussian Process (GP) to determine the distribution of priors, thus, the belief about the shape of F over a set of points is a multivariate Gaussian with means M and covariance K. In particular, a Matérn was adopted as a kernel for K with standard coefficients ($\nu = 5/2$, $\alpha = 1x\ 10^{-6}$). The next zone in X for the evaluation is determined by means of the Acquisition Function (AF), which combines the mean and the covariance of the GP and plays the role of compass in the trade-off between exploitation and exploration searches. The Upper Confidence Bound (UCB) described in equation 9 was chosen as AF, in which θ is the hyperparameter for the tuning between exploitation and exploration phase, set at 0.5.

$$AF = M(x) + \theta\ K(x) \qquad (9)$$

The iterative workflow of the implemented algorithm can be summarized in four main points: i) an initial number of randomly generated sets is evaluated and used to calculate the objective function; ii) the prior are fit to those points according to the GP; iii) the objective function is evaluated with the set which optimizes the acquisition function over the GP model; iv) priors are updated to posteriors with the latest evaluated set of points.

According to the set of target properties described in the previous section, the objective function is defined so that the optimal surrogate mixture lies on a weighted Pareto's frontier with minimum Euclidean distance from the target properties of the objective fluid, which is the SAE-5W30 in this work. The complete expression of the objective function is reported in equation 10, in which e is the relative error ((surrogate – SAE-5W30)/SAE-5W30 x 100) for each target property, W is the respective weight tuned by the Authors in line with the analysis of intermediate results in order to give more emphasis to the targets that are harder to capture. It must be underlined that the last term at the right-hand-side of equation 10, is meant to weight the number of components of the mixture in order to limit the computing effort in simulations that use the surrogate mixture. The error e_N is defined as the ratio between the number of components selected by the optimization algorithm and the database size, namely the maximum number of available components, multiplied by 100. For the sake of clarity, the set of the tuned algorithm is summarized in Table 5.

$$F = 100 - \left(\frac{\sqrt{W_1 \cdot e_\rho^2}}{\sqrt{\sum_i W_i}} + \frac{\sqrt{W_2 \cdot e_\lambda^2}}{\sqrt{\sum_i W_i}} + \frac{\sqrt{W_3 \cdot e_C^2}}{\sqrt{\sum_i W_i}} + ..\right.$$

$$+ \frac{\sqrt{W_4 \cdot e_{TNB}^2}}{\sqrt{\sum_i W_i}} + \frac{\sqrt{W_5 \cdot e_{TFP}^2}}{\sqrt{\sum_i W_i}} + .. \qquad (10)$$

$$\left. + \frac{\sqrt{W_6 \cdot e_\mu^2}}{\sqrt{\sum_i W_i}} + \frac{\sqrt{W_7 \cdot e_N^2}}{\sqrt{\sum_i W_i}}\right)$$

Table 5. Full setup of the tuned Bayesian optimization methodology for oil surrogate mixtures application.

Parameter	Value
GP Kernel	Matérn
ν Matérn	5/2
α Matérn	1.0 x 10-6
θ UCB	0.5
Num. of random search pt.s	150
Num. of maximum iter	300
[W₁,W₂,W₃,W₄,W₅,W₆,W₇]	[1.1, 1.0, 1.0, 1.3, 1.0, 1.3, 1.0]

Diffusion and evaporation models

The above-described methodology is used to obtain the composition of a lubricant oil and to model a set of its properties. The lubricant oil composition and its properties are then passed as inputs to a diffusion and evaporation model, which is now described. This model is used to address the evaporation and the diffusion between the lubricant oil components, while it allows to analyze the properties dependency on the temperature and the pressure of the system. The Authors propose a numerical model which allows to study the physical phenomena of mass and heat transfer inside an engine cylinder. In particular, considering a hydrogen fuelled engine, lubricant oil evaporation needs to be accounted for because the temperature at the liner wall is higher with respect to a traditional DI engine. This is due to the short flame quenching distance typical of hydrogen. With these regards, a large bore hydrogen fuelled DI engine, which is representative of a heavy duty or marine engine, is considered. The code is able to model the mutual diffusion between the components of a multicomponent liquid (namely the lubricant oil), while accounting for its evaporation due to the heat transfer with both the solid wall and the in-cylinder gas. The computational domain is composed by a solid wall and the liquid lubricant layer which are separated by a solid – liquid interface (SLI) and a moving boundary to resolve lubricant oil evaporation. The discretization of the computational domain (Figure 1) is performed with a one – dimensional approach, along the radial dimension.
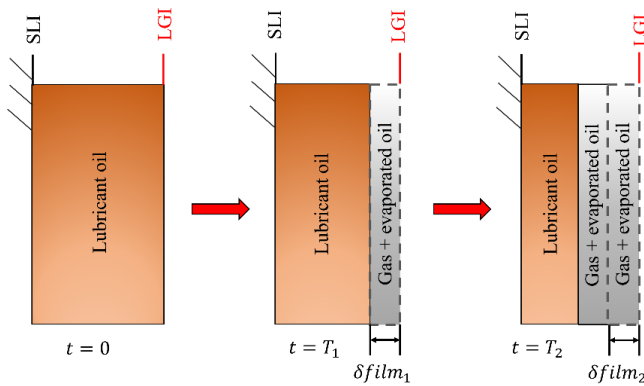

Figure 1. Schematic representation of the computational domain and of the lubricant oil evaporation.

The model base grid has been determined and optimized after stabilty and computational time considerations and assuming that the mass and heat transfer phenomena take place in a few dozens of microns. Once the base grid size is established, the model time step is obtained according to the Courant – Friederichs – Lewy (CFL) condition for thermal diffusion. The one-dimensional Fourier's equation (equation 11) governs the heat transfer for both the solid and liquid phases, where α is the thermal diffusion coefficient. The temperature of the liner wall boundary adjacent to the coolant itself is kept constant, while the in-cylinder gas temperature is taken from an *OpenWAM* model which is briefly described later in this work. The mass transfer between the lubricant oil components is modelled with the second Fick's diffusion law (equation 12) under the assumptions of i) thin liquid film, ii) absence of viscous dissipations, iii) lubricant oil components dilute mixture. The liquid diffusion coefficient (D_L) is estimated through the empirical correlation of Siddiqi and Lucas [35].

$$\frac{dT}{dt} = \alpha \frac{d^2T}{dx^2} \qquad (11)$$

$$\frac{d\xi}{dt} = D_L \frac{d^2\xi}{dx^2} \qquad (12)$$

Results

In this section the results of both the surrogate optimization process and the diffusion and the evaporation simulations are presented. As previously mentioned in the methodology section, at first an analysis is performed to establish the minimum number of surrogate components and to determine the quality of the components, then, the influence of the temperature is studied in terms of the surrogate composition. Three different temperatures are tested with the aim to reproduce three different engine operative conditions, leading to three different surrogates. Then, a unique surrogate is obtained by weight averaging the components of the three different surrogates. Lastly, this surrogate is used in the oil diffusion and evaporation model in comparison with a pseudo-pure liquid approach.

Number of surrogate components

At first, a maximum of 20 components is set for the surrogate formulation (Table 2), then, simulation tests have been performed to reduce the maximum number while keeping the match with the real SAE 5W30 oil. Figure 2 and Figure 3 show the comparison between the achieved errors and objective function with dependence on the number of components used. Different pure fluid databases are tested for each number of components, however for sake of brevity only the best cases are reported. In particular, the last 8 component surrogate is composed by pentane, pentadecane, eicosane, pentacosane, triacontane, pentatriacontane, tetracontane and pentatetracontane. The objective function keeps around ≈ 95 % accuracy for each test, demonstrating that a good fit is achieved despite the limited number of pure fluids available to formulate the mixture. Also, the errors on properties keep under 10%. It must be underlined that oil additives are not taken into account, only the base lubricant oil is modelled. There are many different types of additives which are key for targeting and enhancing some properties. Viscosity and thermal conductivity show the smallest percentages errors, which are significantly lower than the 5% for every temperature. Density and liquid heat capacity errors keep almost constant and around ≈ 5%. Higher errors are shown for the flash point and the NBT, which rise up to around ≈ 10%.
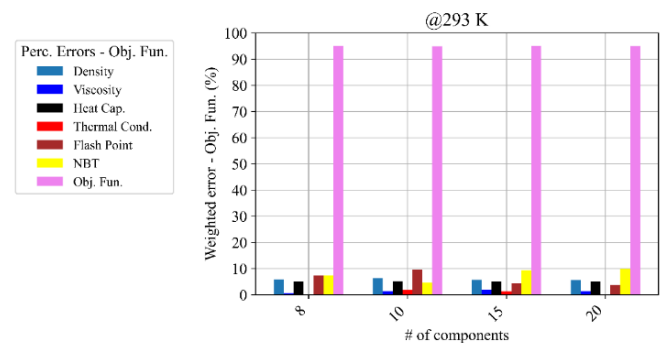

Figure 2. Comparison between errors and objective functions achieved through different tests with different number of components.

Figure 3 shows in detail the influence of the number of components on the calculated properties with respect to the target ones, highlighting that thermal conductivity, viscosity and NBT are the more affected by the database reduction. Instead, thermal conductivity shows a weaker dependency on the database reduction, while it almost doesn't affect the errors on density and liquid heat capacity.
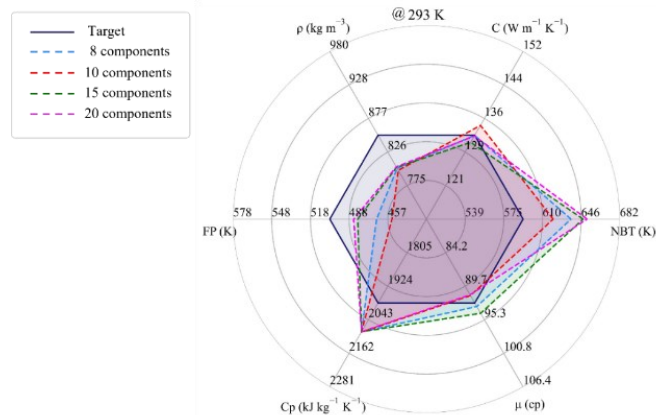
Figure 3. Spider plot that compares the target values of the chosen properties and the calculated by means of the optimization process with different number of components.
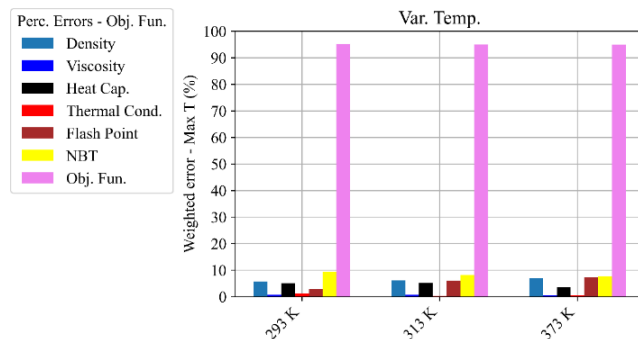

Figure 4. Histogram that shows the percentages errors of the calculated properties with respect to the targets and the achieved objective function at 293 K, 313 K and 373 K.

Concerning the proposed methodology to optimize the composition of the multicomponent surrogate mixture of engine oils, the main advantages can be resumed in the following three points: i) relatively low optimization time (the exploration of a 20-dimension solution domain require few minutes on a standard technology laptop); ii) thanks to the exploration-exploitation trade-off and the statics nature of the technique, the algorithm ensure the localization of the global maximum of the objective function instead of local maxima or 'good enough' solutions as those typically returned by heuristic techniques; iii) optimized percentage of different components enhance the accuracy of the results e.g., the initial mass fraction of hydrocarbons provided to chemical kinetics simulations. On the other hand, some disadvantages must be taken into account: i) the choice of the objective function and of the properties to capture is arbitrary, so the final surrogate; ii) the choice of the pure components in the database is not fully free. Indeed, it strongly depends on the final application e.g., in the case of chemical kinetics simulations of oil ignition, the user must verify the availability of reliable kinetics mechanisms for the molecules included in the database; iii) due to the statistics nature of the method, successive runs of the code with the same tuning parameters lead to different results. Thus, the user must pay care on the convergence process.

Surrogates at different temperatures

Once the components of the surrogate are fixed, the optimization algorithm has been run at different temperatures. The different temperatures aim to reproduce different operative conditions for the lubricant oil on the cylinder liner: for instance, low, medium and high load conditions are associated to the three different temperatures which are respectively 293 K, 313 K and 373 K. Figure 4 shows that the surrogates are able to describe the selected properties with errors below 10 % for every tested temperature, while the objective function keeps around ≈ 95 % of confidence.

In the dilution and evaporation model a unique surrogate is needed to account for the evolution, during the simulation, of its properties and to evaluate its evaporation. Then, a new surrogate is achieved by averaging, with optimized weights, and normalizing the components of the three previous. The first three surrogates are called "base surrogates" and the last one is called "derived surrogate". At first, the weights for the base surrogates are all imposed equal to one, the derived surrogate is found and then its properties are again calculated at every temperature and compared to the targets. Then, the higher errors coupled with the temperature at which they are found are stored and the weights are adjusted in order to minimize these errors by increasing the weight which multiplies the base surrogate at the selected temperature. After some iterations, the weights have been set at 1.2, 1.0, 1.5 for the three base surrogates calculated at 293 K, 313 K and 373 K. Figure 5 shows the composition of the base and derived surrogates while Figure 6 shows the percentages errors and the objective functions for the derived surrogate at different temperatures. In general, compositions for the 313 K and 373 K cases follow the same trend except for C35 and C40, where a ≈ 10 % difference is noticeable. On the other hand, the 293 K surrogate shows a different distribution among all the components, with respect to the other cases, but for C5 and C45, which are comparable. This is due, for instance, to the fact that viscosity is strictly dependent on temperature in a way that the higher the temperature, the lower it is the viscosity gradient with respect to the temperature itself. As previously mentioned, C5 and C45 percentages keep almost constant for each case because of the need to balance high viscosity and density, given by high carbon number hydrocarbons, with the target thermal conductivity, flash point and NBT which are more affected by lower carbon number hydrocarbons. The stronger differences in terms of composition are observable for C15 and C20: in particular, C20 is not present in the 293 K surrogate. The achieved confidence on the properties is acceptable being the errors comparable between the two cases except for viscosity. The error on the viscosity increases for every tested temperature rising beyond the 10 % threshold for 373 K. This is due to the strong dependence of viscosity on the components carbon number (i.e., on the components molecular weight) and on temperature. Despite that, the objective function is always above 90 %.
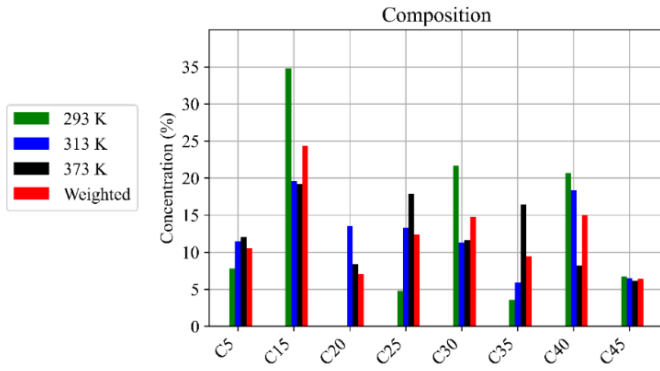
Figure 5. Histograms which show the surrogates composition at 293 K, 313 K and 373 K and the resulting derived averaged composition of the surrogate based on the first three.
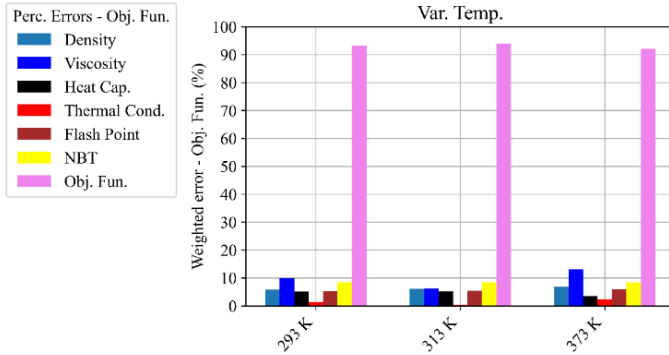

Figure 6. Histograms that show the percentages errors and the objective function for a surrogate derived from weighted averaging the components of the surrogates achieved for each temperature.

A comparison between the properties calculated with the base and the derived surrogates is showed in Figure 7. In particular, the blue polygon is composed by the target properties values, while the green and the red dashed polygon are composed by the calculated properties with the base and the derived surrogates respectively. The 293 K and the 373 K are affected by higher errors with respect to the 293 K and to the target, as the polygons shapes suggest.
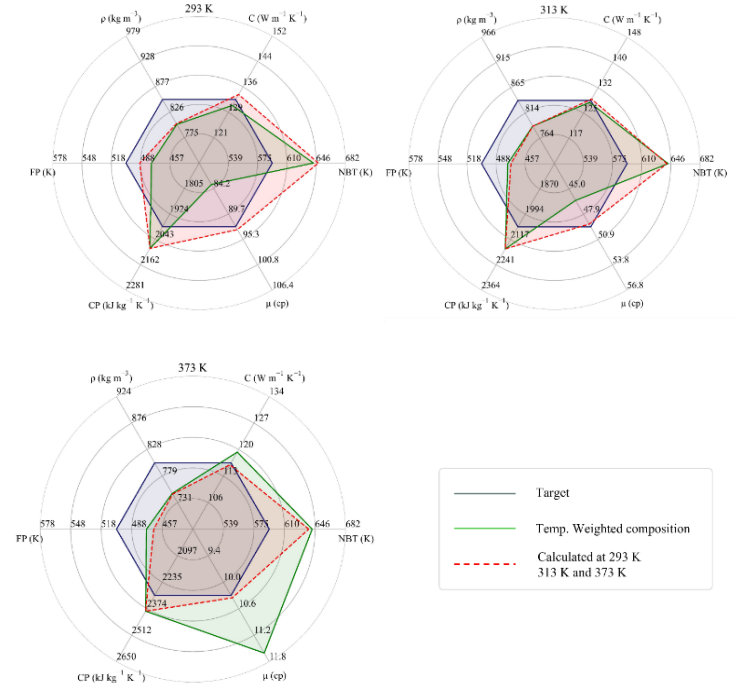

Figure 7. Spider plots which show the comparison between the properties directly calculated through the three different surrogates at 293 K, 313 K and 373 K respectively and the properties calculated with the surrogate whose components are the components of the first three surrogates, once they are weighted and averaged.

Engine geometry and reference conditions for the lubricant oil evaporation test case

The hydrogen fuelled engine geometrical data and the operative conditions in the present work are listed in Table 6 and based on the marine lean-burn spark ignition (SI) engine of the paper [36]. The operative parameters are selected to simulate a high engine load condition, which is critical for oil evaporation. With these regards, engine speed is set at 1500 rpm with a boost pressure of 1.8 bar and an air temperature of 308 K. Engine walls and coolant temperature are maintained at 363 K. The same condition is tested with both a multicomponent and pseudo-pure liquid approaches. The fuel is pure hydrogen, while the lubricant oil is modelled with a SAE 5W30 synthetic oil whose properties have already been discussed earlier. The initial lubricant layer is assumed to be equal to 4 μm. The boundary and initial conditions of pressure and temperature inside the combustion chamber are obtained through a free, open-source one-dimensional gas-dynamic code, namely *OpenWAM*.

In the next sections the results from the 1D model of heat and mass transfer between the lubricant oil, the combustion chamber and the cylinder walls are presented for both the pseudo-pure and the multicomponent approaches. The 1D simulations start from 560 crank angle degree (CAD), i.e. 1.5 CAD before the inlet valves closing (IVC), while they end at 780 CAD, i.e. 60 CAD after top dead center (ATDC) or when the lubricant oil is fully evaporated. This range allows to account for the thermal behavior of the lubricant film during compression and combustion phases.

Table 6. Specification of the hydrogen fuelled engine and operative conditions.

Parameters	Specifications
Displacement	4313 cm3
Bore x Stroke	170 mm x 190 mm
Geometric Compression Ratio	12:1
Engine speed	1500 rpm
Boost Pressure	1.8 bar
Intake air temperature	308 K
Coolant temperature	363 K

Pseudo-pure SAE 5W30

Figure 8 and Figure 9 show, respectively, the lubricant oil temperature profiles along different measure points on the thickness and the thickness evolution during simulation time. The film temperature rises with the combustion chamber temperature during the compression stroke. Also, a change in the curves slope is noticeable around 730 CAD, after the spark event and after the heat from combustion is able to affect the wall temperature. With the pseudo-pure approach, the lubricant oil layer fully evaporates during combustion. Figure 9 shows the temperature profile at different time steps: the x-axis refers to the film distance from the cylinder liner wall. Temperature starts to noticeably rise from 620 CAD, after the first half of compression stroke. At ≈ 746 CAD, the film adjacent to the combustion chamber reaches ≈ 1000 K and almost instantly evaporates.
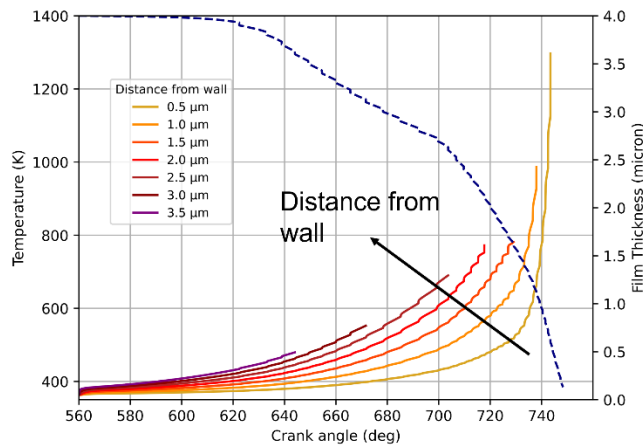

Figure 8. Lubricant oil layer temperature evolution during time at different distances from the cylinder liner wall for the pseudo-pure approach.
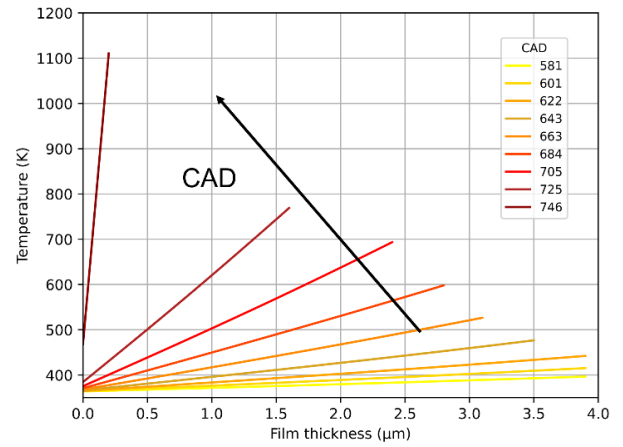

Figure 99. Lubricant oil layer temperature evolution during time at different angles from the cylinder liner wall for the pseudo-pure approach.

Multicomponent SAE 5W30 and comparison

The results of the multicomponent approach are presented in this subsection. Figure 10 shows the profile temperatures against simulation time, while Figure 11 shows the evolution of the temperature with respect to the film thickness at different CADs. Also in this case, temperature suddenly rises up after the compression top dead center and after the spark event, with a delay due to the heat transfer characteristic time. The temperature of the cell at a distance of 0.5 μm from the cylinder liner wall stabilizes at approximately 1200 K, being this film portion close to the cylinder liner wall and being the temperature at the wall a fixed boundary condition. The lubricant film does not fully evaporate in the multicomponent approach: this is due to the fact that the evaporation rates of the heavier hydrocarbons are much lower than those of the lighter hydrocarbons.
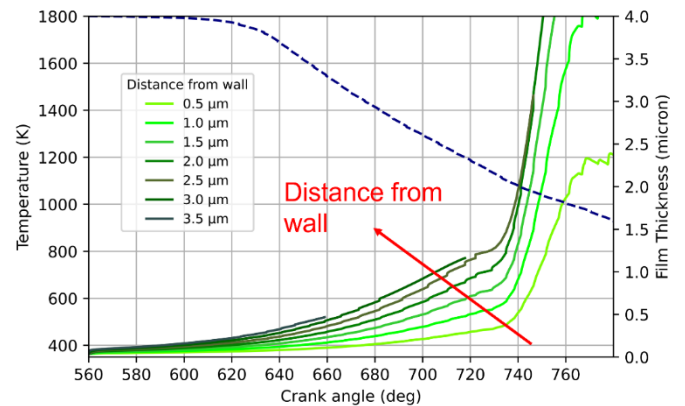

Figure 100. Lubricant oil layer temperature evolution during time at different distances from the cylinder liner wall for the multicomponent approach
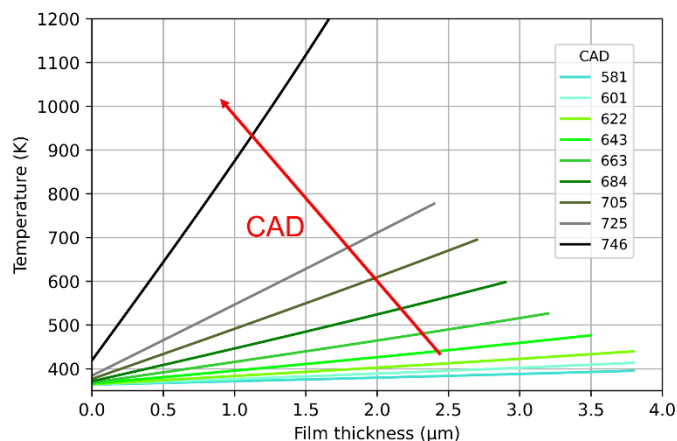
Figure 111. Lubricant oil layer temperature evolution during time at different angles from the cylinder liner wall for the multicomponent approach

Figure 12 shows a comparison of the lubricant oil viscosity evolution during the simulation for the pseudo-pure and the multicomponent approaches. The lubricant layer viscosity significantly decreases with the heat up of the lubricant layer due to the high temperature of a hydrogen combustion, which let viscosity drops below 10 cP. In the multicomponent case, lubricant does not fully evaporate because of the evaporation of the lighter components and the consequent diffusion from the inner cells towards the combustion chamber slows down evaporation. Also, the layer viscosity drops even lower with respect to the pseudo-pure case due to the higher reached temperatures.
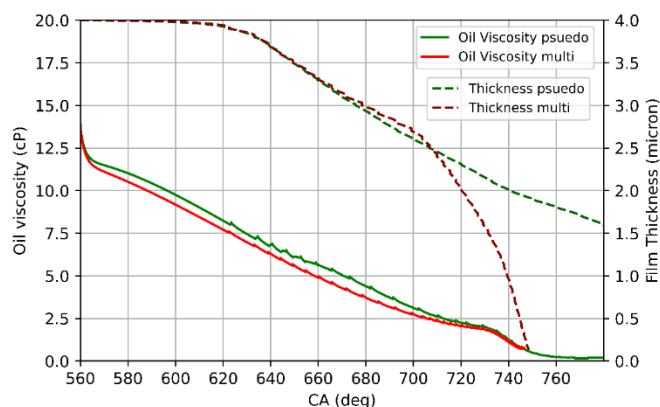

Figure 12. Lubricant oil layer viscosity and thickness comparisons during the simulation for the pseudo-pure and the multicomponent approaches.

Conclusions

This paper deals with the numerical description of the thermal behavior of commercial engine oils under hydrogen combustion conditions in order to simulate the derating of key properties and evaluate the oil evaporation. In this work, the optimization algorithm provides a 1D oil diffusion and evaporation model with a multicomponent mixture of different hydrocarbons which mimics the SAE5W30 commercial oil. This composition is determined by defining some key lubricant oil properties such as viscosity, density, flash point, thermal conductivity, normal boiling temperature, liquid specific heat and the associated weights and an objective function to maximize. The one-dimensional simulations are performed both with a multi-component and a pseudo-

05/31/2023

pure liquids approach. The 1D model is able to predict the heat transfer from the combustion chamber to the lubricant oil and to cylinder liner and the mass transfer between the lubricant components in the multi-component approach. Also, the model allows to evaluate the lubricant oil evaporation and the evolution of some lubricant key properties with the film temperature. The simulations results show that the pseudo-pure liquid fully evaporates during the combustion phase, while the heavier components lower evaporation rates does not allow the complete film evaporation in the multicomponent case. This methodology can provide useful information about the lubricant oil behavior when the lubricant layer is subjected to high temperatures, which are typical of a hydrogen fuelled engine due to the hydrogen short flame quenching distance. Also, lubricant oil droplet could be dispersed in the combustion chamber, thus autoigniting and generating PM. Since hydrogen combustion has water as a product and the hydrogen flame quenching distance is short, future works could address the possible lubricant oil – water dilution once also water evaporation and its effect are considered. Besides, the proposed methodology allows to study and compare the behavior of different lubricant oil under different engine operative conditions.

References

1. Saliba, G., Saleh, R., Zhao, Y., Presto, A. A. at al., "Comparison of Gasoline Direct-Injection (GDI) and Port Fuel Injection (PFI) Vehicle Emissions: Emission Certification Standards, Cold-Start, Secondary Organic Aerosol Formation Potential, and Potential Climate Impacts," Env. Sci. Tech., 51(11), 6542–6552, 2017, doi:10.1021/acs.est.6b06509.
2. Hoffmann, G., Befrui, B., Berndorfer, A., Piock, W. et al., "Fuel System Pressure Increase for Enhanced Performance of GDi Multi-Hole Injection Systems," SAE Int. J. Engines 7(1):519-527, 2014, doi:10.4271/2014-01-1209.
3. Zhu, S., Hu, B., Akehurst, S., Copeland, C. et al., "A review of water injection applied on the internal combustion engine," Energy Conv. Manag., 184, 139-158, 2019, doi:10.1016/j.enconman.2019.01.042.
4. Folkson, R., "Alternative Fuels and Advanced Vehicle Technologies for Improved Environmental Performance", 2014, ISBN: 978-0-85709-522-0.
5. Randolph, E., Fieseler, K., Conway, G., Alger, T. et al., "The Effects of EGR Composition on Combustion Performance and Efficiency," SAE Int. J. Adv. & Curr. Prac. in Mobility 3(1):250-261, 2021, doi:10.4271/2020-01-2052.
6. Alvarez, C. E. C., Couto, G. E., Roso, V. R., Valle, R. M., "A review of prechamber ignition systems as lean combustion technology for SI engines," App. Therm. Eng., 128, 107-120, 2018, doi:10.1016/j.applthermaleng.2017.08.118.
7. Xie, H., Chen, T., Yu, W., Wang, X. et al., "Study on spark assisted compression ignition (SACI) combustion with positive valve overlap at medium–high load," App. Energy, 101, 622-633, 2013, doi:10.1016/j.apenergy.2012.07.015.
8. Falfari, S., Cazzoli, G., Mariani, V., Bianchi, G. M., "Hydrogen Application as a Fuel in Internal Combustion Engines," Energies, 16, 2545-2557, 2023, doi:10.3390/en16062545.
9. Onorati, A., Payri, R., Vaglieco, B., Agarwal, A. K. et al., "The role of hydrogen for future internal combustion engines," Int. J. Eng. Res., 23(4), 529-540, 2023, doi:10.1177/14680874221081947.
10. Rouleau, L., Duffour, F., Walter, B., Kumar, R., et al., "Experimental and Numerical Investigation on Hydrogen Internal Combustion Engine", SAE Tech. Paper 2021-24-0060, 2021, doi:10.4271/2021-24-0060

11. Rezael, R., Hayduk, C., Fandakov, A., Rieß, M., et al., "Numerical and Experimental Investigations of Hydrogen Combustion for Heavy-Duty Applications", SAE Tech. Paper 2021-01-0522, 2021, doi:10.4271/2021-01-0522

12. Raza, M., Chen, L., Leach, F. and Ding, S., "A Review of Particulate Number (PN) Emissions from Gasoline Direct Injection (GDI) Engines and Their Control Techniques," Energies, 11, 6, 2018, doi:10.3390/en11061417.

13. Miller, A. L., Stipe, C., Habjan, M. C. and Ahlstrand, G. G., "Role of lubrication oil in particulate emissions from a hydrogen-powered internal combustion engine," Env. Sci. Tech., 41, 19, 6828-6835, 2007, doi:10.1021/es070999r.

14. Pardo-García, C., Orjuela-Abril, S. and Pabón-León, J., "Investigation of Emission Characteristics and Lubrication Oil Properties in a Dual Diesel–Hydrogen Internal Combustion Engine," Lubricants, 10(4), 59, 2022, doi:10.3390/lubricants10040059.

15. Yu, S. and Min, K., "Effects of the oil and liquid fuel film on hydrocarbon emissions in spark ignition engines," J. Auto. Eng., 216(9), 759-771, 2002, doi:10.1243/09544070260340853.

16. Zhang, Q., Kalva, V., and Tian, T., "Modeling the Evolution of Fuel and Lubricant Interactions on the Liner in Internal Combustion Engines," SAE Technical Paper 2018-01-0279, 2018, doi:10.4271/2018-01-0279.

17. Mariani, V., Bianchi, G. M., Cazzoli, G., Falfari, S., "A one-dimensional model for the motor oil-fuel dilution under gasoline engine boundary conditions," E3S Web Conf., 2020, doi:10.1051/e3sconf/202019706004.

18. Williams, P., Abbass, M., Andrews, G., and Bartle, K., "The influence of PAH contamination of Lubricating Oil on Diesel Particulate PAH Emissions," SAE Technical Paper 890825, 1989, https://doi.org/10.4271/890825.

19. Zhu, Y., Jia, M., Niu, B., Tian, J. et al., "Development of diesel surrogates for reproducing the effect of fuel properties on engine combustion and emissions using an optimized decoupling physical–chemical surrogate (DPCS) model," Fuel, 310, 2022, doi:10.1016/j.fuel.2021.122424.

20. Pulga, L., Lacrimini, D., Forte, C., Mariani, V. et al., "Comparison between Conventional and Non-Conventional Computer Methods to Define Antiknock Properties of Fuel Mixtures," Fuels, 3, 217-231, 2022, doi:10.3390/fuels3020014.

21. Mariani, V., Pulga, L., Bianchi, G. M., Falfari, S. et al., "Machine Learning-Based Identification Strategy of Fuel Surrogates for the CFD Simulation of Stratified Operations in Low Temperature Combustion Modes," Energies, 14(15), 2021, doi:10.3390/en14154623.

22. De Renzis, E., Mariani, V., Bianchi, G. M., Falfari, S. et al., "Application of a one-dimensional fuel-oil dilution model coupled with an empirical droplet-to-film formation strategy for predicting in-cylinder oil effects in a direct injection engine," J. of Physics: Conf. S., 2385, 2022, doi:10.1088/1742-6596/2385/1/012063.

23. Lu, S. and Kaplan, I. R., "Characterization of Motor Lubricating Oils and Their Oil–Water Partition," Environ. Forensics, 9(4), 295-309, 2008, doi:10.1080/15275920802119441.

24. Cvengroš, J., Liptaj, T. and Pronayova, N., "Study of polyaromatic hydrocarbons in current used motor oils," Int. J. of Pet. Sci. & Eng., 2(7), 219-226, 2017, doi:10.15406/ipcse.2017.02.00060.

25. Wang, F. C. and Zang, L., "Chemical Composition of Group II Lubricant Oil Studied by High-Resolution Gas Chromatography and Comprehensive Two-Dimensional Gas Chromatography," Energy Fuels, 21(6), 3477–3483, 2007, doi:10.1021/ef700407c.

26. Green, D. W., "Perry's Chemical Engineers' Handbook, Seventh Edition", McGraw-Hill, 1997.

27. Shahabi-Ghahfarokhy, A., Nakhaei-Kohani, R., Amar, M. N. and Hemmati-Sarapardeh, A., "Modelling density of pure and binary mixtures of normal alkanes: Comparison of hybrid soft computing techniques, gene expression programming, and equations of state," J. of Pet. Sci. and Eng., 208, 2022, doi:10.1016/j.petrol.2021.109737.

28. Dadgostar, N. and Shaw, J. M., "A predictive correlation for the constant-pressure specific heat capacity of pure and ill-defined liquid hydrocarbons," Fluid Phase Equilib., 313, 211-226, 2012, doi:10.1016/j.fluid.2011.09.015.

29. Vidal, M., Rogers, W. J., Holste, J. C. and Mannan, M. S., "A review of estimation methods for flash points and flammability limits," Process Saf. Prog., 2004, 23, 47-55, doi:10.1002/prs.10004.

30. Royal Society of Chemistry, ChemSpider, [Online]. Available: https://www.chemspider.com. [Accessed February 2023].

31. Slavinskaya, N. A., Zizin, A. and Aigner, M., "On Model Design of a Surrogate Fuel Formulation," J. Eng. Gas Turbines Power, 132, 2010, doi:10.1115/1.4000593.

32. Samimi Abianeh, O., Chen, C. P. and Cerro, R. L., "Batch Distillation: The Forward and Inverse Problems," Ind. Eng. Chem. Res., 51(38), 12435–12448, 2012, doi:10.1021/ie300710s.

33. Soave, G., "Equilibrium constants from a modified Redlich-Kwong equation of state," Chem. Eng. Sci., 1972, 27(6), 1197-1203, doi:10.1016/0009-2509(72)80096-4.

34. Bruno, T. J. and Huber, M. L., "Evaluation of the Physicochemical Authenticity of Aviation Kerosene Surrogate Mixtures. Part 1: Analysis of Volatility with the Advanced Distillation Curve," Energy Fuels, 24(8), 4266–4276, 2010, doi:10.1021/ef100496j.

35. Siddiqi, M. and Lucas, K., "Correlations for prediction of diffusion in liquids," Canadian J. of Chem. Eng., 64, 839-843, 1986.

36. Sapra, H., Godjevac, M., De Vos, P., Van Sluijs, W. et al., "Hydrogen-natural gas combustion in a marine lean-burn SI engine: A comparitive analysis of Seiliger and double Wiebe function-based zero–dimensional modelling," Energy Conv. Manag., 207, 2020, doi:10.1016/j.enconman.2020.112494.

Declaration of interests

The authors declare that they have no known competing financial interests or personal relationships that could have appeared to influence the work reported in this paper.

Acknowledgements

05/31/2023